Received: 16 November 2021 | Revised: 5 July 2022 | Accepted: 6 July 2022

DOI: 10.1111/ejn.15808

RESEARCH REPORT

EJN European Journal of Neuroscience FENS WILEY

Largely unaffected auditory and visual sensory processing phenotypes in the evoked potentials of Fmr1 KO2 mice

Renate Kat | **Martien J. H. Kas**

Groningen Institute for Evolutionary Life Sciences (GELIFES), University of Groningen, Groningen, The Netherlands

Correspondence
Martien J.H. Kas, Groningen Institute for Evolutionary Life Sciences (GELIFES), University of Groningen, Nijenborgh 7, 9747 AG, Groningen, The Netherlands.
Email: m.j.h.kas@rug.nl

Funding information
ZonMW TOP, Grant/Award Number: 91216021

Edited by: Sophie Molholm

Abstract

Sensory sensitivity symptoms are common in autism spectrum disorders and fragile X syndrome. Mainly in the auditory modality, disturbed processing has been found in both fragile X patients and the corresponding genetic mouse model, the Fmr1 knockout mouse. Here, we tried to replicate the auditory deficits and assess whether also visual processing is affected, using electroencephalography readouts under freely behaving conditions in the second-generation Fmr1 knockout mice. No differences between wild-type and knockout animals were found in single auditory and visual evoked potentials in response to pure sine tones and full-field light flashes. Visual sensory gating was enhanced in the early but not the late components of the evoked potentials, but no changes were found in auditory sensory gating. The higher harmonics of the synchronisation response to flickering visual stimuli seemed to be reduced with 10, but not 20 or 40 Hz, stimulation. However, this effect was not reproduced in an independent second cohort of animals. No synchronisation differences were found in response to a chirp stimulus, of which the frequency steadily increased. Taken together, this study could not reproduce earlier reported increased amplitudes in auditory responses, nor could it convincingly show that synchronisation deficits found to be present in the auditory modality also existed in the visual modality. The discrepancies within this study as well as between various studies assessing sensory processing in the Fmr1 KO raise questions about the external validity of these phenotypes and warrant careful interpretation of these phenotypes.

KEYWORDS
autism spectrum disorder, EEG, event-related potential (ERP), sensory processing

List of abbreviations: AEP, auditory evoked potential; ASD, autism spectrum disorder; EEG, electroencephalogram; EMG, electromyogram; ERP, event-related potential; FXS, fragile X syndrome; ISI, inter-stimulus interval; ITI, inter-trial interval; ITPC, inter-trial phase consistency; KO, knockout; KO2, second-generation knockout; LED, light-emitting diode; N1, first negative peak of the ERP; N1P2, amplitude from the N1 to the P2; Non-REM, non-rapid eye movement; P1, first positive peak of the ERP; P1N1, amplitude from the P1 to the N1; P2, second positive peak of the ERP; PPI, prepulse inhibition; VEP, visual evoked potential; VSSR, visual steady state response; WT, wildtype.

1 | INTRODUCTION

The Fmr1 gene knockout (KO) mouse is a widely used model for Fragile X syndrome (FXS), the most common monogenetic form of intellectual disability and autism spectrum disorders (ASD; Kazdoba et al., 2014). Sensory processing deficits are being increasingly recognised as a core feature of ASD (Baum et al., 2015; Sinclair et al 2017), and hypersensitivity to sensory stimuli is a well-known feature of FXS (Baranek et al., 2002; Rais et al., 2018). Using electroencephalogram (EEG) recordings, increased amplitudes in the response to auditory stimuli, the auditory evoked potentials (AEPs), have been shown in patients, specifically in the first negative wave (N1, Castrén et al., 2003; Ethridge et al., 2019; Knoth et al., 2014; Van der Molen et al., 2012a, 2012b). However, these amplitude changes were not always replicated (Ethridge et al., 2016). Additionally, FXS patients were found to generate a less strong synchronisation to oscillating auditory stimuli. When presenting a so called 'chirp' stimulus, in which the frequency of amplitude modulation of the stimulus gradually increases, patients showed higher alpha power at the onset of the stimulus compared to healthy controls, but no increases in the high gamma power, possibly as a result of already heightened baseline gamma power (Ethridge et al., 2017). Similarly, in patients the inter-trial phase consistency (ITPC) in response to the chirp stimulus was increased at alpha frequencies around onset but reduced when the stimulus reached gamma frequencies of 30–60 Hz (Ethridge et al., 2017; 2019). Visual processing has been less extensively studied, and both increased as well as unaffected visual evoked potentials (VEPs) amplitudes have been found (Knoth et al., 2014; Rigoulot et al., 2017; Van der Molen et al., 2012a).

In the Fmr1 KO mouse model, a recent meta-analysis showed sensory hyposensitivity in auditory and pain processing, but results so far were inconsistent for somatosensory and olfactory sensitivity (Kat et al., 2022). In the visual modality, deficits were found in the optomotor reflex and visual depth perception (Felgerolle et al., 2019). Using EEG, Fmr1 KO animals were found to show altered responses at the level of the auditory brainstem response; however, these results were quite inconsistent between studies (El-Hassar et al., 2019; Kim et al., 2013; Rotschafer et al., 2015). In 2013, the first study assessing cortical activity in response to auditory stimulation reported increased spiking responses (Rotschafer & Razak, 2013). In line with this result, increased AEP amplitudes were also found in KO animals. Some studies found the amplitude differences between KO and wild-type (WT) animals to be largest on temporal recording locations (Jonak et al., 2020), but surprisingly, the differences have also been shown to be present only on frontal recording locations (Lovelace et al., 2018; Wen et al., 2019). One study found increased amplitudes in response to 14 kHz, but not 23 kHz stimuli (Kulinich et al., 2020), and one study did not find any amplitude differences between the genotypes (Lovelace et al., 2016). The synchronisation to chirp stimuli and stimuli of a stable frequency showed lower gamma frequency power and ITPC in KO animals, similar as in patients (Jonak et al., 2020; Kozono et al., 2020; Lovelace et al., 2018; Pirbhoy et al., 2020). However, one study also showed higher ITPC in the high gamma frequencies in KO animals (Lovelace et al., 2020). In the VEPs, no N1 amplitude differences were found in juvenile Fmr1 KO rats (Berzhanskaya et al., 2016). However, some changes have been shown in higher-order visual processing. Perceptual experience-induced oscillations in the V1 were reduced (Kissinger et al., 2020). In an oddball paradigm, KO mice showed similar levels of stimulus-specific adaptation but stronger mismatch responses (Pak et al., 2021).

In the current study, we tried to replicate and extend the understanding of auditory and visual processing in the Fmr1 KO2 mouse, the second-generation Fmr1 KO model (Mientjes et al., 2006). In addition to single AEPs and VEPs, we assessed both visual and auditory sensory gating, measured as the reduction in amplitude of the response to the second of two identical stimuli. This paradigm is an analogue of the regularly used prepulse inhibition paradigm that measures sensorimotor gating and has previously revealed deficits in both FXS patients as well as first-generation Fmr1 KO mice (Frankland et al., 2004; Hessl et al., 2009; Hodges et al., 2019; Olmos-Serrano et al., 2011; Yuhas et al., 2011). Lastly, as the synchronising deficits to auditory stimuli have been quite consistently shown in both patients as well as the first-generation KO mice, but were never studied in the visual modality, we assessed whether Fmr1 KO2 mice also show deficits in neuronal synchronisation to visual stimuli.

2 | MATERIALS AND METHODS

2.1 | Mice

Original breeding females from the Fmr1 KO2 line (Mientjes et al., 2006) on a C57/BL6J (Envigo) background were generously provided by the Netherlands Institute for Neuroscience (Amsterdam, NL). The initial experiments were performed with a cohort of 22 male mice (10 WT, 12 KO). Retesting of the visual steady-state response (VSSR) was performed with a second cohort of 23 male mice (12 WT, 11 KO). To obtain the animals from the first cohort, heterozygous females were crossed

with WT males, which resulted in nests with $Fmr1^{-/y}$ (KO) and $Fmr1^{+/y}$ (WT) littermates. For the second cohort, heterozygous females were crossed with both WT and knockout male mice, which also generated KO and WT littermates. Considering that Fmr1 is an x-linked gene and male experimental animals get the y, not x, chromosome from their fathers, paternal genotype should have minimal effects on the experimental animals. DNA for genotyping was extracted from ear clips using a lysis buffer (100 mM Tris pH 8.0, 200 nM NaCl, 5 nM ethylenediaminetetraacetic acid) with proteinase K (0.2 mg/ml). Reverse transcription polymerase chain reaction was performed using the following primers: reverse transgene (5′ GCC TCA CAT CCT AGC CCT CTA C 3′), reverse internal control (5′ CCC ACA AAG TTGA TTC CCC AGA 3′) and forward transgene/internal control (5′ CCC ACT GGGA GAG GAT TAT TTG GG 3′).

Mice were weaned at 3–4 weeks of age. Until surgery, the animals were housed with four male animals from different nests and mixed genotypes (2 KO and 2 WT) in a cage. For the first cohort, surgery took place at 12 weeks of age, whereas for the second cohort surgery took place at 8 weeks of age. Mice were kept on a 12:12 light–dark cycle with ad libitum access to food and water. All experiments were performed in accordance with the European Directive 2010/63/EU and according to a research protocol approved by the local animal welfare body. All efforts were made to minimise discomfort of the experimental animals.

2.2 | Electroencephalography

EEG recordings were performed using the wireless multichannel TaiNi EEG system (Tainitec, London, UK). The animals underwent stereotactic EEG implantation surgery under isoflurane anaesthesia (0.8–1.5%, in oxygen-enriched air) and local lidocaine anaesthesia. Custom-designed implants (ND & Associates, Berkshire, UK) with six epidural screw electrodes (0.7 mm, Antrin miniature specialties, Fallbrook, USA) were implanted. One electrode was placed above the right prefrontal cortex (bregma +2.6 mm anterior, −1.6 mm lateral), and bilateral electrodes were placed above the primary visual (bregma −4 mm posterior, ±3.0 mm lateral) and the primary auditory cortex (bregma −2.5 mm posterior, ±3.5 mm lateral). A reference electrode was placed centrally on the cerebellum. In the second cohort of animals, left visual and auditory electrodes were not screws but silver ball-tip electrodes. The signals from the ball-tip electrodes were not used in the analysis of the current study. Two electromyogram (EMG) electrodes were placed under the neck muscles. Both the electrodes and the implant were fixated on the skull using dental cement (RelyX Unicem Aplicap cement, 3 M, Minneapolis, USA). Pain killing was applied by a subcutaneous injection of Carprofen (5 mg/kg) both before the start of the surgery and 24 h post surgery.

After surgery, the animals were pair-housed with mixed genotypes in semi-separating cages. In the middle of the cage, a see-through plexiglass separator, with a fissure at head height, was placed. This separator allowed for visual, auditory, olfactory and some extent of somatosensory contact between pair-housed animals but prevented cage mates from damaging each other's implant. In the second week of operative recovery, the animals were habituated to handling, short head fixation by holding the implant with plyers (necessary for connecting the transmitter) and connecting and wearing the transmitter. EEG recordings started after a recovery period of at least 14 days.

EEG signals were recorded with a sampling rate of 19,525 Hz or 1085 Hz, respectively, for the first and second cohorts, and 9700 Hz high-pass and 0.35 Hz low-pass online filters in the TaiNiLive software (v1.3, Tainitec, London, UK). Activity of the animals during EEG recordings was recorded via passive infrared (PIR) motion sensors with the Micro1401 (Cambridge Electronic Devices, Cambridge, UK). Digital pulses were sent to the EEG system every minute for later synchronisation of the EEG data with the movement sensor data using Spike2 software (v10, Cambridge Electronic Devices, Cambridge, UK). Visual and auditory recordings were performed between 15 and 20 weeks of age for the first cohort of animals and at 10 weeks of age for the second cohort of animals.

2.3 | Visual evoked potentials

For the recording of VEPs, mice were put inside a computer-controlled custom-built light-emitting diode (LED)-illuminated sphere in which mice were able to move freely (Van Diepen et al., 2013; Figure 1a). The sphere (30-cm diameter) was coated with high-reflectance paint that spread light produced by a ring of white monochromatic LEDs at the top of the sphere. A baffle prevented the mice from looking directly into the LEDs. Stimulation paradigms were programed in Spike2 and controlled the sphere via the Micro1401. VEP recordings were performed during the light phase, and background light levels in the sphere were 2 lx. In several sessions, spread over three to four non-consecutive days mice were exposed to multiple paradigms including: single VEP, paired flash, VSSR and a visual chirp. Recording sessions had a maximum duration of 2 h,

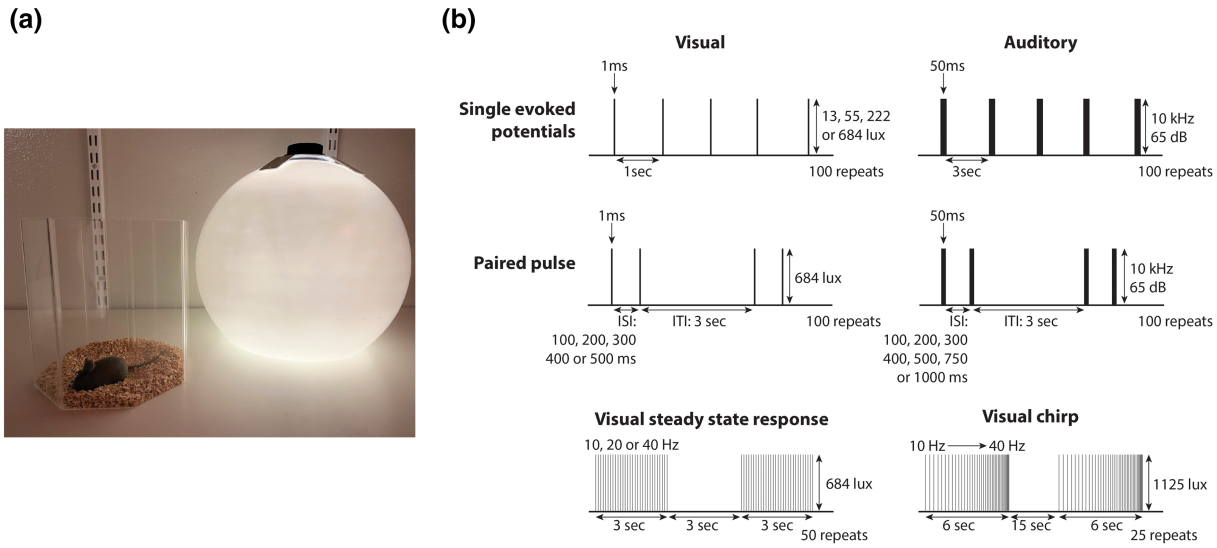

FIGURE 1 **Setup for visual stimulus presentation and sensory paradigm characteristics.** The sphere used for visual stimulus presentation is presented in Figure 1a. Mice were put into an arena they could freely explore, after which the sphere was placed around this arena in such a way that the mouse was now inside the sphere. Characteristics of the various sensory paradigms used in the current study are presented in Figure 1b

after which the mice were placed back into their home cage. Mice were allowed to habituate to the recording cage inside the sphere for 15 min before the start of the first paradigm of each day, and between two paradigms tested on the same day was always a 5-min rest period in which mice remained in the recording cage. Characteristics of the various paradigms are also presented in Figure 1b.

Single VEP One hundred light flashes of 1 ms were presented at a rate of 1 Hz. In separate blocks, four different light intensities were tested, namely 13, 55, 222 and 684 lx. Between the blocks of different intensities was a 1-min interval.

Paired flash Two identical flashes were presented with a short inter-stimulus interval (ISI). One hundred pairs of flashes were presented with a 3-s inter-trial interval (ITI) between the pairs. The tested ISIs between two stimuli were 100, 200, 300, 400 and 500 ms. Between the blocks of different ISIs was a 1-min interval. All flashes were 684 lx.

VSSR Flashes of 1 ms were presented at different frequencies in 3-s pulse trains. Fifty trains were presented with a 3-s ITI between the trains. Frequencies of 10, 20 and 40 Hz were tested. Between the blocks of different frequencies was a 1-min interval. All flashes were 684 lx.

Visual chirp Twenty-five trains of 6 s with a sweep of increasing frequencies were presented. The frequency within the train increased from 10 to 40 Hz with steps of 1 Hz. Four 1-ms flashes of each frequency were presented. All flashes were 1125 lx.

2.4 | Auditory event-related potentials

For the recording of AEPs, mice were put into recording cages individually. Speakers (Ultrasonic Dynamic Speaker Vifa, #60108, Avisoft Bioacoustics, Nordbahn, Germany) were placed in between the recording cages. Pure sine tones were presented at 65 ± 3 dB over a 50-dB background noise level. Audio files of the paradigms were built in Avisoft SASlab Pro (v5.2, Avisoft Bioacoustics, Nordbahn, Germany). AEP recordings were performed during the dark phase. Mice were allowed to habituate for 15 min before the start of the first paradigm. A single AEP and a paired tone paradigm were presented on the same day with a 5-min rest period in between. AEPs were not recorded on the same day as the VEPs. Characteristics of the various paradigms are also presented in Figure 1b.

Single AEP One hundred 10 kHz tones with a duration of 50 ms were presented with an ISI of 3 s.

Paired tone Two itones were presented with a short ISI. One hundred pairs of tones were presented with a 3-s ITI between the pairs. The tested ISIs between two stimuli were 100, 200, 300, 400, 500, 750 and 1000 ms. Between the blocks of different ISIs was a 1-min interval.

2.5 | Event-related potential analysis

First, recordings were manually checked to exclude recordings with periods of sleep. For sleep detection, recordings were screened for the presence of periods

where the PIR motion detector did not pick up non-specific locomotor activity. Periods without locomotor activity that coincided with stimulus presentation were checked for the presence of non-rapid eye movement (non-REM) sleep, as defined by high-amplitude delta (<4 Hz) waves, so called slow waves, in the frontal EEG signal in combination with an absence of activity in the EMG signal. One WT animal from the second cohort was excluded from the analysis because of sleep during stimulus presentation.

Data processing was performed in Matlab (v2018a & v2018b, MathWorks, Natick, MA, USA). For single event-related potential (ERP) and paired pulse paradigms, data were downsampled to 781 Hz. Using threshold-based exclusion, signal-loss artefacts were removed from the data. Subsequently, gaps in the data were interpolated using the resample function (Signal Processing Toolbox), which fills in missing datapoints on a straight line between the last datapoint before and the first datapoint after the gap. Trials with interpolated stretches longer than 10 ms were excluded from the analysis. The data were high-pass filtered at 0.5 Hz and low-pass filtered at 100 Hz with a fourth-order Butterworth filter. After filtering, threshold-based artefact detection, with a threshold of five standard deviations from the mean, was applied, and trials with artefacts were excluded from the analysis. For one KO animal, the data in the 100-ms ISI version of the paired flash paradigm had to be excluded because more than 25% of the trials in this condition were rejected for either signal loss or threshold exceeding artefacts. ERPs were extracted from 100 ms before stimulus onset to 300 and 400 ms after stimulus onset, respectively, for auditory and visual stimuli. Trials were averaged (when applicable per light intensity or ISI) and baseline corrected using a baseline window from −100 to 0 ms. For the analysis of the VEPs, data recorded from the V1 electrodes were used, whereas for the analysis of the AEPs, data recorded from the A1 electrodes were used. ERPs were averaged over the right and left auditory or visual electrodes for the first batch of animals but not for the second batch of animals as the ball-tip electrodes implanted on the left hemisphere were not used.

For the paired pulse paradigms, amplitude ratios between the conditioning (first) and test (second) stimulus were calculated. For the paired tone, a P1N1 amplitude was calculated by subtracting the minimum value between 0 and 300 ms (N1) from the maximum value between 0 and 300 ms (P1). As the VEPs had a slightly more complex shape, a P1N1 amplitude, as well as a N1P2 amplitude, was calculated. P1 was defined as the maximum between 0 and 100 ms, N1 as the minimum before 200 ms, and P2 as the maximum between 100 and 300 ms. The P1N1 (and N1P2) ratios were calculated by dividing the amplitude from the test stimulus by the amplitude of the conditioning stimulus.

The visual chirp and steady-state paradigms were analysed using time-frequency analysis with Morlet wavelet convolution. The data from the first cohort were downsampled from 19,525 to 355 Hz, whereas the data from the second cohort were kept at the original 1085 Hz. Because both sampling frequencies are well above the Nyquist frequency of 200 Hz (double the highest frequency of interest), the difference in sampling frequency between the two cohorts does not affect the analysis (Cohen, 2014; Shannon, 1949). Similar artefact rejection procedures were applied as described for the ERPs, with the exception that trials were only rejected if they had interpolated stretches of over 100 ms. In the steady-state paradigm, one WT had to be excluded from the 40-Hz condition and one KO had to be excluded from the 20-Hz condition because of exceeding the maximum of 25% rejected trials. In the chirp, one WT and two KO animals had to be excluded because of exceeding the maximum of 25% rejected trials. In the second cohort, one WT animal in the 10-Hz condition and one WT and one KO animals in the 20-Hz condition had to be excluded because of exceeding the rejection threshold. The data were high-pass filtered at 0.5 Hz and low-pass filtered at 150 Hz with a fourth-order Butterworth filter. Trials were extracted from the data from 3 s before to 6 s after stimulus onset and were baseline corrected with a 100-ms baseline before stimulus onset. Morlet wavelet convolution was applied from 5 to 100 Hz in 0.5 Hz linear steps. The number of cycles increased from 8 to 15 with increasing frequencies. The power was extracted as the squared absolute value from the convolution product, and ITPC was extracted as the angle from the convolution product. Both were averaged over trials. Decibel conversion was applied to the power using a baseline window from 2 to 1 s before stimulus onset.

2.6 | Statistics

Single ERPs, the steady-state response and the chirp response were all analysed using cluster-based permutation analysis (Maris & Oostenveld, 2007). In short, independent *t* test statistics were obtained for every time- or time-frequency point and were clustered over time (and frequency) along adjacent points that reached above the *t* value threshold corresponding to an alpha level of 0.05. The sum of all *t* values in a cluster was used as the cluster statistic. To assess significance of these clusters, a 'null' distribution was created by performing 1000 random permutations between WT and KO animals. Cluster statistics were extracted for every permutation in the same manner

as described above. Both the largest positive and the largest negative clusters from each permutation were used to create two distributions. Clusters in the actual data were considered significant when exceeding the 97.5-percentile threshold for cluster statistic in either the positive or negative distribution. Clusters were reported when $p < 0.2$, where $p < 0.05$ was considered significant. Cluster-based permutation analysis does not have a good level of precision for finding exact onsets and offsets; therefore, borders of the time, as well as time frequency, windows of reported clusters should be interpreted carefully (Sassenhagen & Draschkow, 2019).

For the amplitude ratios of the paired pulse paradigms, one sample t tests (two-sided) were first used on data averaged over both genotypes to test whether significant sensory gating was present at the different ISIs (i.e. amplitude ratios were different from 1). Bonferroni correction was used to correct for testing at multiple ISIs. Mixed effects linear models were used to test the effects of genotype, ISI and possible interactions in RStudio (v1.1453 [R v3.6.3], Boston, MA, USA; lme4 package v1.1–23). Using model comparison based on Akaike Information Criterion, the best model was selected. The following models were found:

Auditory P1N1 ~ genotype + ISI + (1|animalID)
Visual P1N1 ~ genotype * ISI + (1|animalID)
Visual N1P2 ~ genotype + ISI + (1|animalID)

Chi-squared tests were used to determine the statistical significance of the effects, and post-hoc tests were performed using Bonferroni corrections.

The data in the text are presented as mean ± standard deviation. The type of variance plotted in the figures can be found in corresponding figure legends.

3 | RESULTS

3.1 | Single evoked potentials

The animals were presented with single pure sine tones (10 kHz, 50 ms, 65 dB) and single white light flashes (1 ms; 13, 55, 222 and 684 lx) to record evoked potentials. AEPs showed a clear P1–N1 structure with a latency of approximately 20 and 40 ms for the P1 and N1, respectively (Figure 2a). Cluster-based permutation analysis did not reveal genotype differences between WT and KO animals. VEPs had a more complex shape, especially in response to the higher stimulation intensities (Figure 2b). Visual inspection of the waveforms showed multiple fast peaks between approximately 20–80 ms, followed by a negativity starting around 100 ms and a late broad positivity around 200 ms. As with the AEPs, no genotype differences between WT and KO were found (13 lx: ~320–340 ms, $p = 0.11$). AEPs and VEPs also did not show any

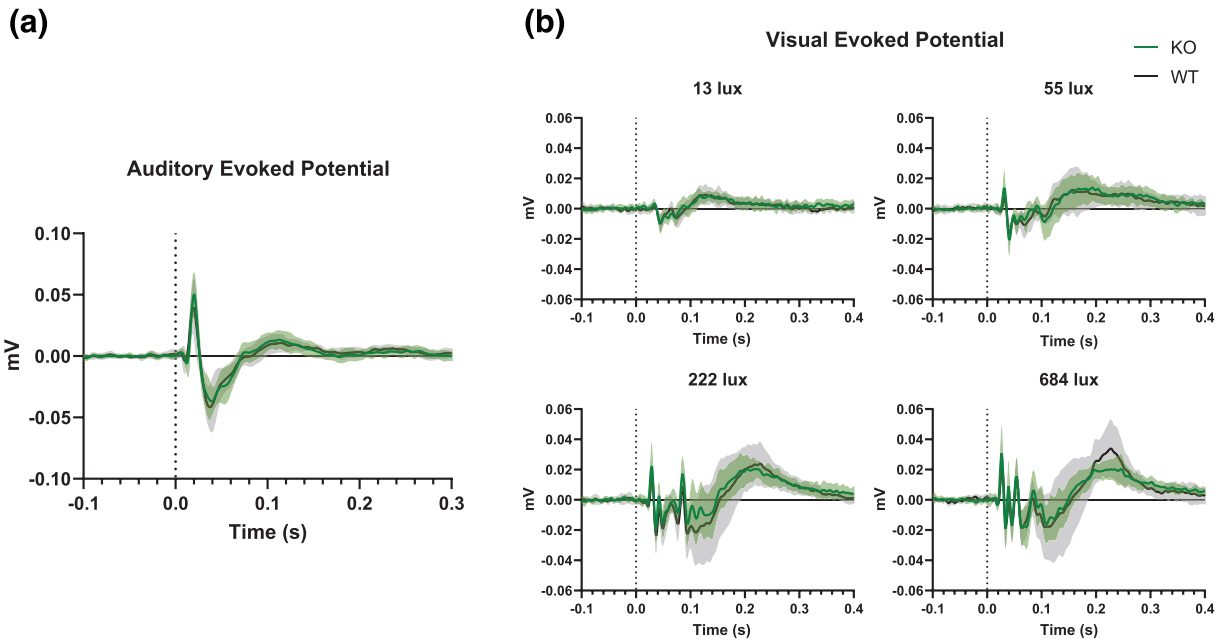

FIGURE 2 **Auditory and visual single evoked potentials.** (a) Auditory evoked potentials were induced by 100 repetitions of a 50 ms 10 kHz tone. (b) Visual evoked potentials were induced by 100 repetitions of a 1 ms flash of 13, 55, 222 and 684 lx. Waveforms were averaged over the right and left auditory or visual cortex. WT: $n = 10$; KO: $n = 12$. The data are presented as a mean with S.E.M. shading.

genotype differences in the frontal electrodes (data not shown).

3.2 | Sensory gating

Using paired pulse paradigms, in which two identical stimuli are presented with a short ISI, sensory gating was assessed. For auditory stimuli, a clear reduction in amplitude in response to the test (second) stimulus was seen in comparison to the conditioning (first) stimulus (Figure 3a). P1N1 amplitudes were calculated for both test and conditioning stimuli by subtraction of the N1 peak value from the P1 peak value. The strength of sensory gating for the different ISIs was expressed as the P1N1 ratio (test P1N1/conditioning P1N1, Figure 3b). When looking at the combined data of WT and KO animals, significant sensory gating was found to be present at all ISIs tested (100 ms: $t_{21} = -27.01$, $p < 0.001$; 200 ms: $t_{21} = -32.40$, $p < 0.001$; 300 ms: $t_{21} = -28.44$, $p < 0.001$; 400 ms: $t_{21} = -17.35$, $p < 0.001$; 500 ms: $t_{21} = -18.15$, $p < 0.001$; 750 ms: $t_{21} = -15.84$, $p < 0.001$; 1000 ms: $t_{21} = -8.50$, $p < 0.001$). Mixed linear modelling showed a significant reduction of sensory gating with longer ISIs ($\chi^2_6 = 658.63$ [$n = 154$], $p < 0.001$). However, there was no main effect of genotype ($\chi^2_1 = 1.89$ [$n = 154$], $p = 0.169$).

For visual stimuli, sensory gating was observed to be less strong. Because of the more complex shape of these evoked potentials, not only the P1N1 ratio was calculated (Figure 3c) but also the N1P2 ratio (Figure 3d), P2 being the broad positivity around 200 ms. When looking at the combined data of WT and KO animals, it was found that for the P1N1 ratio significant gating was only present in

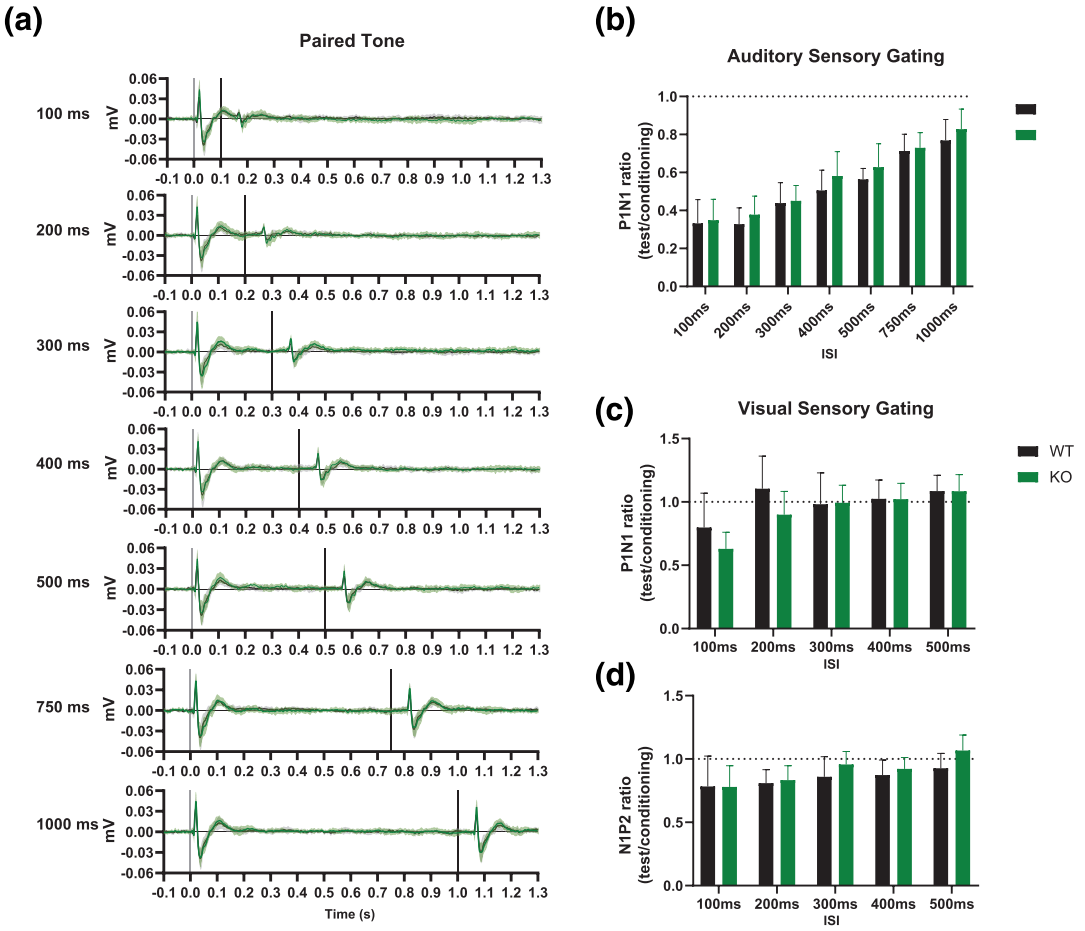

FIGURE 3 **Auditory and visual sensory gating.** (a,b) Auditory and (c,d) visual paired pulse paradigms were presented with ISIs ranging from 100 to 1000 or 100 to 500 ms, respectively. AEP amplitude in the response to the test stimulus (a, gray vertical bar) was reduced compared to the amplitude of the response to the conditioning stimulus (a, black vertical bar). Amplitude ratios were calculated by subtracting the peak amplitude of N1 from P1 or P2 from N1 for both de test and conditioning stimulus and subsequently divide the amplitude of the test stimulus by the amplitude of the conditioning stimulus. Responses from the right and left visual or auditory cortex were averaged. WT: $n = 10$; KO: $n = 12$ (visual-100 ms: $n = 11$). The data are presented as a mean with (a) S.E.M. shading or (b–d) mean ± SD

the 100 ms ISI ($t_{20} = -6.00$, $p < 0.001$). For the P1N1 ratio, both the main effect for genotype ($\chi^2{}_1 = 4.86$ [$n = 109$], $p = 0.027$) and ISI ($\chi^2{}_4 = 82.34$ [$n = 109$], $p < 0.001$) as well as the interaction between the two ($\chi^2{}_4 = 13.69$ [$n = 109$], $p = 0.008$) were significant. Post hoc comparisons with Bonferroni correction revealed significantly more gating in KO animals with ISIs of 100 and 200 ms but not at longer ISIs. In the N1P2 ratio,

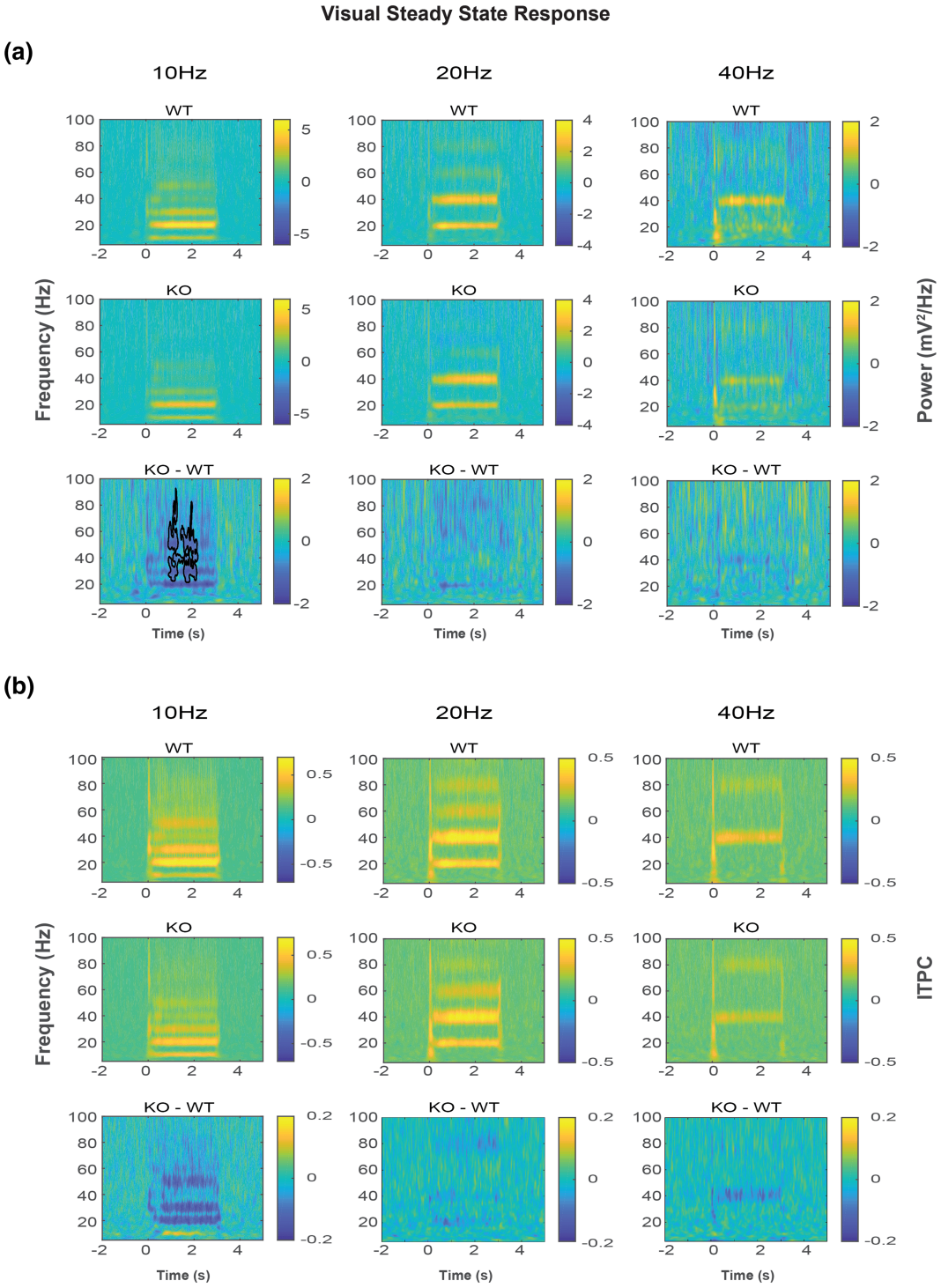

FIGURE 4 **Visual steady state response.** Three-second trains of flashes were presented at 10, 20 and 40 Hz. (a) Power and (b) intertrial phase consistency (ITPC) in response to these stimuli were obtained by performing Morlet wavelet convolution from 5 to 100 Hz, with 0.5-Hz steps. Decibel conversion baseline correction was performed for the power with −2 to −1 s as baseline window. Significant clusters ($p < 0.05$) are outlined in black. Responses from the right and left visual cortex were averaged. WT: $n = 10$ (20 Hz: $n = 9$); KO: $n = 12$ (40 Hz: $n = 11$)

combined data of the WT and KO animals revealed significant sensory gating for ISIs up to 400 ms (100 ms: $t_{20} = -5.02$, $p < 0.001$; 200 ms: $t_{21} = -7.68$, $p < 0.001$; 300 ms: $t_{21} = -3.01$, $p = 0.034$; 400 ms: $t_{21} = -4.51$, $p < 0.001$). For the N1P2 ratio, only the main effect of ISI was significant ($\chi^2_4 = 42.48$ [$n = 109$], $p < 0.001$), and no differences between the genotypes were found ($\chi^2_1 = 2.83$ [$n = 109$], $p = 0.092$).

4 | NEURONAL SYNCHRONISATION

The ability of the cortex to synchronise to an external stimulus was assessed using neuronal synchronisation paradigms. In the visual steady-state paradigm, the animals were presented with 3-s trains of flickering light of 10, 20 or 40 Hz. Time-frequency analysis revealed increased power in response to the stimuli in both the primary stimulation frequency bands, as well as the power bands of the higher harmonics for all stimulation frequencies in both genotypes (Figure 4a). For the 10-Hz stimulation, the highest power was not found in the primary stimulation frequency but in the first higher harmonic of 20 Hz. When plotting the difference in power response between WT and KO animals (Figure 4a, bottom row), a clear pattern of reduced synchronisation power in the KO animals was seen for stimuli of 10, but not 20 and 40 Hz. Two clusters of significantly reduced power in Fmr1 KO animals were found in the high-frequency ranges above 30 Hz between approximately 1 and 1.5 s post stimulus (Figure 4a, $p = 0.042$) and between 1.5 and 2.2 s ($p = 0.032$; ~ 0.5–1 s/40–90 Hz: $p = 0.062$; ~ 2.4–3 s/30–100 Hz: $p = 0.082$). Despite large differences in power between the genotypes in the 20-Hz frequency band, this difference did not reach significance because of a large variation between animals, which became evident when plotting the power over time per frequency band (supporting information Figure S1). The phase of the responses was assessed by looking at the ITPC, a measure for the consistency in phase between different trials within animals. No differences in phase consistency were found between WT and KO animals (Figure 4b and supporting information Figure S2). Because the reduction in synchronisation power in the KO mice was found to be so specific (only present in the higher harmonics of 10-Hz stimulation), we aimed to assess the robustness of the effect by trying to replicate it in an independent cohort of mice. Lower power responses were in this cohort seen with 20 Hz instead of 10-Hz stimulation (supporting information Figure S3–S5; power in response to 20-Hz stimulation: ~ 0.4–3.0 s/20 Hz: $p = 0.022$; ~ 2.5–3.0 s/60–80 Hz: $p = 0.154$). To test whether the differences between cohorts were a result of using only one recording electrode in the second cohort, we reanalysed the data of the first cohort using only the screw electrode on the right hemisphere. Contrary to the second cohort, again a reduced synchronisation to the 10-Hz stimulus in the KO mice was visible, although it did not represent a statistically significant difference (supporting information Figure S6; ~ 1.5–2.2 s/30–80 Hz: $p = 0.076$).

In addition to steady-state stimuli, the animals were also presented with chirp stimuli, in which the frequency of the flashes within the stimulus train was not stable but increased from 10 to 40 Hz in 6 s. Both genotypes showed synchronisation to these stimuli, but no differences between the genotypes were found in power (Figure 5a) nor ITPC (Figure 5b).

5 | DISCUSSION

Sensory processing deficits have been hypothesised to partly underlie the behavioural symptoms of ASD (Baum et al., 2015; Thye et al., 2018). In this study, we aimed to replicate earlier reported auditory processing deficits in the Fmr1 KO model. Additionally, we also assessed visual processing to further expand the understanding of sensory processing deficits in this model. In contrast to earlier findings in the mouse model (Felgerolle et al., 2019; Jonak et al., 2020; Lovelace et al., 2018; Pirbhoy et al., 2020; Wen et al., 2019) and to the clinical phenotype (Baranek et al., 2002; Ethridge et al., 2016; 2019; Rais et al., 2018), no robust sensory processing deficits were found in the auditory nor the visual modality using the second-generation Fmr1 KO genetic model.

Different elements of sensory processing were assessed using various stimulation paradigms. In the single ERPs, previously reported increased N1 amplitudes in the AEP could not be replicated, nor did we find any alterations in VEP amplitudes. Literature on the N1 amplitude increase is, however, not very consistent, with some studies reporting differences only on either the auditory or the frontal cortex (Jonak et al., 2020; Lovelace et al., 2018; Wen et al., 2019), only in response to tones of specific frequencies (Kulinich et al., 2020) or reporting no differences at all (Lovelace et al., 2016). Three large methodological differences between the present study and the previous studies might explain the lack of an AEP phenotype in the current study. Firstly, most of previous studies used broadband noise as stimuli, whereas here 10-kHz pure sine tones were used, which evoke activation of more specific subsets of auditory neurons. Secondly, the older age of the animals in the current study (15–20 weeks) compared to previous studies (3–12 weeks)

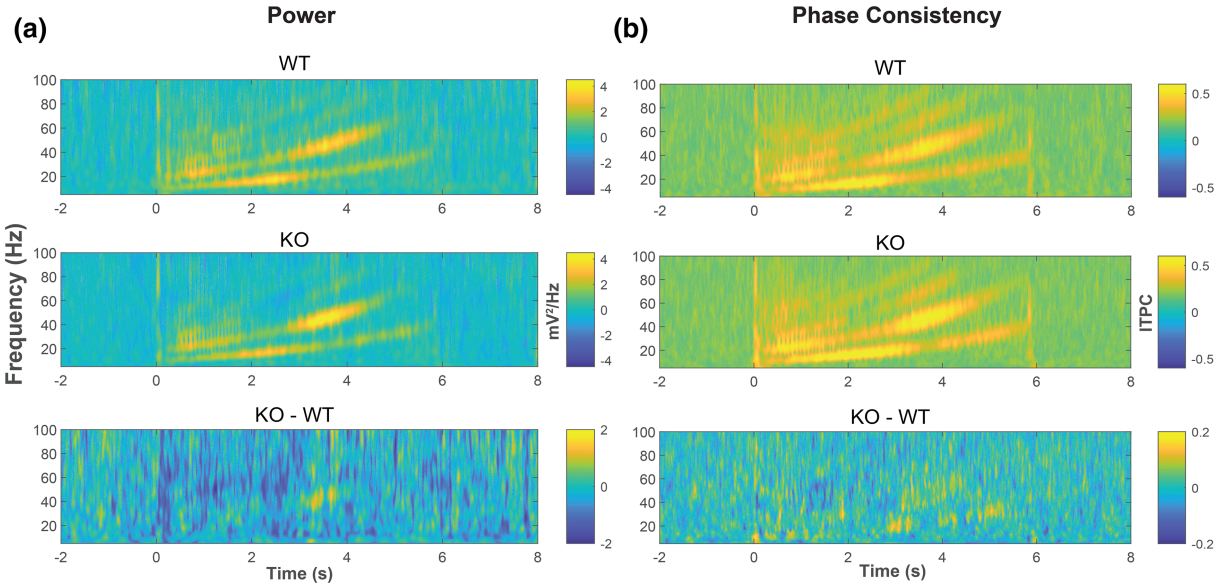

FIGURE 5 **Visual chirp.** Trains of light flashes with increasing frequency were presented. In 6 s, the frequency increased from 10 to 40 Hz. (a) Power and (b) intertrial phase consistency (ITPC) in response to these stimuli were obtained by performing Morlet wavelet convolution from 5 to 100 Hz, with 0.5-Hz steps. Decibel conversion baseline correction was performed for the power with −2 to −1 s as baseline window. Responses from the right and left visual cortex were averaged. WT: $n = 9$; KO: $n = 10$

could explain discrepancies. Although, Wen et al. (2019) did not show any developmental effects on the differences between genotypes when testing animals at multiple time points between 3 and 8 weeks, the phenotype might change in more adult stages. Lastly, in the current study, the second generation of the KO model was used (Mientjes et al., 2006), whereas previous studies assessing sensory processing used the first-generation mouse model (The Dutch-Belgian Fragile X Consortium et al., 1994). Contrary to the first-generation model, in the second-generation model not only the protein but also the mRNA is absent. It remains to be studied if the absence of the mRNA causes alterations in the functional phenotypes, like sensory processing and behaviour. However, if differences between the models exist, more severe phenotypes rather than milder phenotypes would be expected in the second-generation KO model (because of the total absence of Fmr1 protein *and* mRNA). Taken together, previously reported ERP amplitude alterations in the Fmr1 KO models might only be present at certain (early) developmental stages and specific experimental conditions.

In the second paradigm, sensory gating was assessed to investigate the integration of repeated stimuli. Auditory sensory gating was present at all ISIs tested, but no differences between the genotypes were found. This was unexpected, as alterations in sensorimotor gating, measured by the prepulse inhibition (PPI), have been shown in first-generation KO mice, as well as in patients (Frankland et al., 2004; Hessl et al., 2009; Hodges et al., 2019; Olmos-Serrano et al., 2011; Yuhas et al., 2011). However, it is difficult to directly compare sensory gating to PPI, as different processing pathways might be involved. In addition to the sensory systems, PPI also involves motor activity and it has been shown that because of the aversive intensity of the stimuli, also the amygdala and the inferior colliculus can contribute to PPI (Howland et al., 2007; Wan & Swerdlow, 1997). To our knowledge, paired pulse paradigms have not yet been tested before in patients or Fmr1 KO models. More studies are needed before sound conclusions can be drawn about sensory gating in the Fmr1 KO models.

As gamma synchronisation deficits in response to auditory stimuli have been shown repeatedly in both patients (Ethridge et al., 2017, 2019), as well as in KO mice and rats (Jonak et al., 2020; Kozono et al., 2020; Lovelace et al., 2018; Pirbhoy et al., 2020); the last two paradigms assessed whether these deficits extended to the visual modality. Inconsistent results were found when looking at steady-state visual synchronisation, as two independent cohorts of mice showed genotype differences in response to different stimulation frequencies. There were two important differences between the two cohorts which might explain the discrepancies in genotype effects. Firstly, the mice of the second cohort were younger, being tested at 10 instead of 15–20 weeks, which could explain the differences if the phenotypes are not stable over time. Secondly, in the second cohort, the

VSSR was performed as the second paradigm on the first recording day, whereas in the first cohort, the VSSR was performed as the third paradigm on the second recording day and after the animals had also been recorded in 48-h home-case baseline recordings. Differences in prior exposure to the recording setup could influence results because of, for example, differences in stress or attention levels of the animals during the VSSR recordings. Further experiments are needed to test which factors explain the discrepancy between the cohorts. Nevertheless, is it clear that the synchronisation deficit in the visual modality is not very robust and shows low external validity, as it is sensitive to changes in methodological and experimental conditions. Together, this study did not show strong evidence that synchronisation deficits extend to the visual modality. However, further studies will be required to confirm that visual deficits are also not present in younger mice and the first-generation KO model. Additionally, VSSR and visual chirp paradigms have unfortunately not yet been tested in patients. Performing these experiments will increase the understanding of the wider range of sensory processing deficits associated with FXS.

Taken together, the current study seems to suggest little sensory processing deficits in the Fmr1 KO2 mice using EEG-based assessments. However, there are certain technical limitations that need to be taken into consideration when evaluating the results. First of all, the current study used epidural electrodes. These electrodes have relatively high translational value because of their similarity to epidermal clinical recordings; however, they only record global neuronal activity and the spatial resolution of these type of measurements is low as a consequence of volume conduction. Recent studies using laminar probes found various visual processing deficits specifically in the more superficial layers of the cortex (Kissinger et al., 2020; Pak et al., 2021). Because of volume conduction, visual as well as auditory ERPs were also present in the signals of all recording electrodes, but the amplitudes were highest in the electrodes above the corresponding sensory cortex. As not enough electrodes were present to perform source localisation analyses, which could have provided insight into the origin of various components of the ERPs, we analysed the ERPs only on the corresponding primary sensory cortices. Recording the EEG with higher spatial and cortical-layer specificity might reveal genotype differences that could not be picked up with the current recording method. Second, regarding the sensory stimuli that were used, it is important to point out the different nature of the auditory and visual stimuli. Where the pure sine tones evoke responses in smaller subsets of A1 neurons (Guo et al., 2012), the flash stimuli evoke more broad responses in the V1 (Funayama et al., 2016; Land et al., 2019). Unfortunately, in the current visual stimulation setup where animals are moving freely, we are limited to full-field flash stimuli. Further developing this setup, in order to be able to also present more complex visual stimuli of, for example, specific spatial frequency tunings or orientations, could further the understanding of visual processing deficits in the Fmr1 KO models. Third, we may have tested too little animals to detect an effect. However, the sample size of the current study was comparable to other studies which did find ERP amplitude changes (Jonak et al., 2020; Kulinich et al., 2020; Lovelace et al., 2018), making it unlikely that the lack of phenotypes was because of the study being underpowered. Because power calculation methods are not available for the type of statistics that was used and substantial methodological differences exist with the experiments of available effect size estimates, a priori power calculations were not performed and insufficient power cannot be excluded. Lastly, both the current and previous studies have all been performed in male mice. Although FXS is more prevalent in males, also females are affected by FXS, and it is therefore important to also include female mice in future research.

When using the Fmr1 KO models to study sensory processing deficits in FXS, it is important to be aware of the robustness and translatability of the different phenotypes. Based on literature, the auditory-evoked gamma synchronisation deficits seem to have both high robustness and translatability (Ethridge et al., 2017; 2019; Jonak et al., 2020; Kozono et al., 2020; Lovelace et al., 2018; Pirbhoy et al., 2020). On the other hand, the visual synchronisation deficit found in the current study showed low robustness as it could not be replicated in an independent cohort of mice. As little is known about visual processing functioning in patients, it remains to be assessed whether patients show visual synchronisation deficits. The ERP amplitude increases that are shown in the literature (Jonak et al., 2020; Kulinich et al., 2020; Lovelace et al., 2018; Wen et al., 2019) could not be replicated under the specific conditions of this study and thus also seem to be less robust, despite showing translatability to the patient phenotype (Castrén et al., 2003; Ethridge et al., 2019; Knoth et al., 2014; Van der Molen et al., 2012a, 2012b). Taken together, the first-generation Fmr1 KO model can be a good model for auditory synchronisation deficits in FXS. However, the external validity for other sensory phenotypes in both the first- and second-generation models is low, as experimental conditions seem to affect these phenotypes.

ACKNOWLEDGEMENTS

This work was financially supported by a ZonMW TOP grant (grant number 91216021, 2017, awarded to MJK).

The authors thank Pim Drinkenburg and colleagues for the advice on the processing and the analysis of the ERPs.

CONFLICTS OF INTEREST

The authors have no conflicts of interest.

AUTHOR CONTRIBUTIONS

Renate Kat: Conceptualisation, investigation, formal analysis, visualisation, writing – original draft. **Martien J.H. Kas:** Conceptualisation, funding acquisition, supervision, writing – review and editing.

PEER REVIEW

The peer review history for this article is available at https://publons.com/publon/10.1111/ejn.15808.

DATA AVAILABILITY STATEMENT

The data and analysis scripts that support the findings of this study are openly available in the OSF repository at [https://osf.io/cvefk/].

ORCID

Renate Kat https://orcid.org/0000-0001-9584-0034
Martien J. H. Kas https://orcid.org/0000-0002-4471-8618

REFERENCES

Baranek, G. T., Chin, Y. H., Greiss Hess, L. M., Yankee, J. G., Hatton, D. D., & Hooper, S. R. (2002). Sensory processing correlates of occupational performance in children with fragile X syndrome: Preliminary findings. *American Journal of Occupational Therapy*, *56*(5), 538–546. https://doi.org/10.5014/ajot.56.5.538

Baum, S. H., Stevenson, R. A., & Wallace, M. T. (2015). Behavioral, perceptual, and neural alterations in sensory and multisensory function in autism spectrum disorder. *Progress in Neurobiology*, *134*, 140–160. https://doi.org/10.1016/j.pneurobio.2015.09.007

Berzhanskaya, J., Phillips, M. A., Shen, J., & Colonnese, M. T. (2016). Sensory hypo-excitability in a rat model of fetal development in fragile X syndrome. *Scientific Reports*, *6*(July), 1–11. https://doi.org/10.1038/srep30769

Castrén, M., Pääkkönen, A., Tarkka, I. M., Ryynänen, M., & Partanen, J. (2003). Augmentation of auditory N1 in children with fragile X syndrome. *Brain Topography*, *15*(3), 165–171. https://doi.org/10.1023/A:1022606200636

Cohen, M. X. (2014). *Analyzing neural time series data: Theory and practice* (1st ed.). The MIT press.

El-Hassar, L., Song, L., Tan, W. J. T., Large, C. H., Alvaro, G., Santos-Sacchi, J., & Kaczmarek, L. K. (2019). Modulators of Kv3 potassium channels rescue the auditory function of fragile X mice. *Journal of Neuroscience*, *39*(24), 4797–4813. https://doi.org/10.1523/JNEUROSCI.0839-18.2019

Ethridge, L. E., De Stefano, L. A., Schmitt, L. M., Woodruff, N. E., Brown, K. L., Tran, M., Wang, J., Pedapati, E. V., Erickson, C. A., & Sweeney, J. A. (2019). Auditory EEG biomarkers in fragile X syndrome: Clinical relevance. *Frontiers in Integrative Neuroscience*, *13*(October), 1–16. https://doi.org/10.3389/fnint.2019.00060

Ethridge, L. E., White, S. P., Mosconi, M. W., Wang, J., Byerly, M. J., & Sweeney, J. A. (2016). Reduced habituation of auditory evoked potentials indicate cortical hyper-excitability in fragile X syndrome. *Translational Psychiatry*, *6*(4), e787. https://doi.org/10.1038/tp.2016.48

Ethridge, L. E., White, S. P., Mosconi, M. W., Wang, J., Pedapati, E. V., Erickson, C. A., Byerly, M. J., & Sweeney, J. A. (2017). Neural synchronization deficits linked to cortical hyper-excitability and auditory hypersensitivity in fragile X syndrome. *Molecular Autism*, *8*(22). https://doi.org/10.1186/s13229-017-0140-1

Felgerolle, C., Hébert, B., Ardourel, M., Meyer-Dilhet, G., Menuet, A., Pinto-Morais, K., Bizot, J. C., Pichon, J., Briault, S., & Perche, O. (2019). Visual behavior impairments as an aberrant sensory processing in the mouse model of fragile X syndrome. *Frontiers in Behavioral Neuroscience*, *13*-(October), 1–19. https://doi.org/10.3389/fnbeh.2019.00228

Frankland, P. W., Wang, Y., Rosner, B., Shimizu, T., Balleine, B. W., Dykens, E. M., Ornitz, E. M., & Silva, A. J. (2004). Sensorimotor gating abnormalities in young males with fragile X syndrome and Fmr1-knockout mice. *Molecular Psychiatry*, *9*(4), 417–425. https://doi.org/10.1038/sj.mp.4001432

Funayama, K., Hagura, N., Ban, H., & Ikegaya, Y. (2016). Functional organization of flash-induced V1 offline reactivation. *Journal of Neuroscience*, *36*(46), 11727–11738. https://doi.org/10.1523/JNEUROSCI.1575-16.2016

Guo, W., Chambers, A. R., Darrow, K. N., Hancock, K. E., Shinn-Cunningham, B. G., & Polley, D. B. (2012). Robustness of cortical topography across fields, laminae, anesthetic states, and neurophysiological signal types. *Journal of Neuroscience*, *32*(27), 9159–9172. https://doi.org/10.1523/JNEUROSCI.0065-12.2012

Hessl, D., Berry-Kravis, E., Cordeiro, L., Yuhas, J., Ornitz, E. M., Campbell, A., Chruscinski, E., Hervey, C., Long, J. M., & Hagerman, R. J. (2009). Prepulse inhibition in fragile X syndrome: Feasibility, reliability, and implications for treatment. *American Journal of Medical Genetics, Part B: Neuropsychiatric Genetics*, *150*(4), 545–553. https://doi.org/10.1002/ajmg.b.30858

Hodges, S. L., Reynolds, C. D., Nolan, S. O., Huebschman, J. L., Okoh, J. T., Binder, M. S., & Lugo, J. N. (2019). A single early-life seizure results in long-term behavioral changes in the adult Fmr1 knockout mouse. *Epilepsy Research*, *157*(May), 106193. https://doi.org/10.1016/j.eplepsyres.2019.106193

Howland, J. G., Hannesson, D. K., Barnes, S. J., & Phillips, A. G. (2007). Kindling of basolateral amygdala but not ventral hippocampus or perirhinal cortex disrupts sensorimotor gating in rats. *Behavioural Brain Research*, *177*(1), 30–36. https://doi.org/10.1016/j.bbr.2006.11.009

Jonak, C. R., Lovelace, J. W., Ethell, I. M., Razak, K. A., & Binder, D. K. (2020). Multielectrode array analysis of EEG biomarkers in a mouse model of fragile X syndrome. *Neurobiology of Disease*, *138*, 104794. https://doi.org/10.1016/j.nbd.2020.104794

Kat, R., Arroyo-Araujo, M., de Vries, R. B. M., Koopmans, M. A., de Boer, S. F., & Kas, M. J. H. (2022). Translational validity and methodological underreporting in animal research: A systematic review and meta-analysis of the fragile X syndrome (Fmr1 KO) rodent model. *Neuroscience and Biobehavioral Reviews*, *139*, 104722. https://doi.org/10.1016/j.neubiorev.2022.104722

Kazdoba, T. M., Leach, P. T., Silverman, J. L., & Crawley, J. N. (2014). Modeling fragile X syndrome in the Fmr1 knockout mouse. *Intractable & Rare Diseases Research*, *3*(4), 118–133. https://doi.org/10.5582/irdr.2014.01024

Kim, H., Gibboni, R., Kirkhart, C., & Bao, S. (2013). Impaired critical period plasticity in primary auditory cortex of fragile X model mice. *Journal of Neuroscience*, *33*(40), 15686–15692. https://doi.org/10.1523/JNEUROSCI.3246-12.2013

Kissinger, S. T., Wu, Q., Quinn, C. J., Anderson, A. K., Pak, A., & Chubykin, A. A. (2020). Visual experience-dependent oscillations and underlying circuit connectivity changes are impaired in Fmr1 KO mice. *Cell Reports*, *31*(1), 107486. https://doi.org/10.1016/j.celrep.2020.03.050

Knoth, I. S., Vannasing, P., Major, P., Michaud, J. L., & Lippé, S. (2014). Alterations of visual and auditory evoked potentials in fragile X syndrome. *International Journal of Developmental Neuroscience*, *36*, 90–97. https://doi.org/10.1016/j.ijdevneu.2014.05.003

Kozono, N., Okamura, A., Honda, S., Matsumoto, M., & Mihara, T. (2020). Gamma power abnormalities in a Fmr1-targeted transgenic rat model of fragile X syndrome. *Scientific Reports*, *10*(1), 1–9. https://doi.org/10.1038/s41598-020-75893-x

Kulinich, A. O., Reinhard, S. M., Rais, M., Lovelace, J. W., Scott, V., Binder, D. K., Razak, K. A., & Ethell, I. M. (2020). Beneficial effects of sound exposure on auditory cortex development in a mouse model of fragile X syndrome. *Neurobiology of Disease*, *134*(September 2019), 104622. https://doi.org/10.1016/j.nbd.2019.104622

Land, R., Kapche, A., Ebbers, L., & Kral, A. (2019). 32-channel mouse EEG: Visual evoked potentials. *Journal of Neuroscience Methods*, *325*(March), 108316. https://doi.org/10.1016/j.jneumeth.2019.108316

Lovelace, J. W., Ethell, I. M., Binder, D. K., & Razak, K. A. (2018). Translation-relevant EEG phenotypes in a mouse model of fragile X syndrome. *Neurobiology of Disease*, *115*, 39–48. https://doi.org/10.1016/j.nbd.2018.03.012

Lovelace, J. W., Ethell, I. M., Binder, D. K., & Razak, K. A. (2020). Minocycline treatment reverses sound evoked EEG abnormalities in a mouse model of fragile X syndrome. *Frontiers in Neuroscience*, *14*(August), 1–16. https://doi.org/10.3389/fnins.2020.00771

Lovelace, J. W., Wen, T. H., Reinhard, S., Hsu, M. S., Sidhu, H., Ethell, I. M., Binder, D. K., & Razak, K. A. (2016). Matrix metalloproteinase-deletion rescues auditory evoked potential habituation deficit in a mouse model of fragile X syndrome. *Neurobiology of Disease*, *89*, 126–135. https://doi.org/10.1016/j.nbd.2016.02.002

Maris, E., & Oostenveld, R. (2007). Nonparametric statistical testing of EEG- and MEG-data. *Journal of Neuroscience Methods*, *164*(1), 177–190. https://doi.org/10.1016/j.jneumeth.2007.03.024

Mientjes, E. J., Nieuwenhuizen, I., Kirkpatrick, L., Zu, T., Hoogeveen-Westerveld, M., Severijnen, L., Rifé, M., Willemsen, R., Nelson, D. L., & Oostra, B. A. (2006). The generation of a conditional Fmr1 knock out mouse model to study Fmrp function in vivo. *Neurobiology of Disease*, *21*(3), 549–555. https://doi.org/10.1016/j.nbd.2005.08.019

Olmos-Serrano, J. L., Corbin, J. G., & Burns, M. P. (2011). The GABA A receptor agonist THIP ameliorates specific behavioral deficits in the mouse model of fragile X syndrome. *Developmental Neuroscience*, *33*(5), 395–403. https://doi.org/10.1159/000332884

Pak, A., Kissinger, S. T., & Chubykin, A. A. (2021). Impaired adaptation and laminar processing of the oddball paradigm in the primary visual cortex of Fmr1 KO mouse. *Frontiers in Cellular Neuroscience*, *15*(May), 1–15. https://doi.org/10.3389/fncel.2021.668230

Pirbhoy, P. S., Rais, M., Lovelace, J. W., Woodard, W., Razak, K. A., Binder, D. K., & Ethell, I. M. (2020). Acute pharmacological inhibition of matrix metalloproteinase-9 activity during development restores perineuronal net formation and normalizes auditory processing in Fmr1 KO mice. *Journal of Neurochemistry*, *155*, 538–558. https://doi.org/10.1111/jnc.15037

Rais, M., Binder, D. K., Razak, K. A., & Ethell, I. M. (2018). Sensory processing phenotypes in fragile X syndrome. *ASN Neuro*, *10*, 1759091418801092. https://doi.org/10.1177/1759091418801092

Rigoulot, S., Knoth, I. S., Lafontaine, M. P., Vannasing, P., Major, P., Jacquemont, S., Michaud, J. L., Jerbi, K., & Lippé, S. (2017). Altered visual repetition suppression in fragile X syndrome: New evidence from ERPs and oscillatory activity. *International Journal of Developmental Neuroscience*, *59*(March), 52–59. https://doi.org/10.1016/j.ijdevneu.2017.03.008

Rotschafer, S. E., Marshak, S., & Cramer, K. S. (2015). Deletion of Fmr1 alters function and synaptic inputs in the auditory brainstem. *PLoS ONE*, *10*(2), 1–15. https://doi.org/10.1371/journal.pone.0117266

Rotschafer, S. E., & Razak, K. (2013). Altered auditory processing in a mouse model of fragile X syndrome. *Brain Research*, *1506*, 12–24. https://doi.org/10.1016/j.brainres.2013.02.038

Sassenhagen, J., & Draschkow, D. (2019). Cluster-based permutation tests of MEG/EEG data do not establish significance of effect latency or location. *Psychophysiology*, *56*(6), 1–8. https://doi.org/10.1111/psyp.13335

Shannon, C. E. (1949). Communication in the presence of noise. *Proceedings of the IRE*, *37*(1), 10–21. https://doi.org/10.1109/JRPROC.1949.232969

The Dutch-Belgian Fragile X Consortium, Bakker, C. E., Verheij, C., Willemsen, R., van der Helm, R., Oerlemans, F., Vermey, M., Bygrave, A., Hoogeveen, A. T., Oostra, B. A., Reyniers, E., De Boule, K., D'Hooge, R., Cras, P., van Velzen, D., Nagels, G., Martin, J.-J., De Deyn, P. P., Darby, J. K., & Willems, P. J. (1994). Fmr1 knockout mice: A model to study fragile X mental retardation. *Cell*, *78*(1), 23–33. https://doi.org/10.1016/0092-8674(94)90569-X

Thye, M. D., Bednarz, H. M., Herringshaw, A. J., Sartin, E. B., & Kana, R. K. (2018). The impact of atypical sensory processing on social impairments in autism spectrum disorder. *Developmental Cognitive Neuroscience*, *29*(May 2017), 151–167. https://doi.org/10.1016/j.dcn.2017.04.010

Van der Molen, M. J. W., Van der Molen, M. W., Ridderinkhof, K. R., Hamel, B. C. J., Curfs, L. M. G., & Ramakers, G. J. A. (2012a). Auditory and visual cortical

activity during selective attention in fragile X syndrome: A cascade of processing deficiencies. *Clinical Neurophysiology*, *123*(4), 720–729. https://doi.org/10.1016/j.clinph.2011.08.023

Van der Molen, M. J. W., Van der Molen, M. W., Ridderinkhof, K. R., Hamel, B. C. J., Curfs, L. M. G., & Ramakers, G. J. A. (2012b). Auditory change detection in fragile X syndrome males: A brain potential study. *Clinical Neurophysiology*, *123*(7), 1309–1318. https://doi.org/10.1016/j.clinph.2011.11.039

Van Diepen, H. C., Ramkisoensing, A., Peirson, S. N., Foster, R. G., & Meijer, J. H. (2013). Irradiance encoding in the suprachiasmatic nuclei by rod and cone photoreceptors. *FASEB Journal*, *27*(10), 4204–4212. https://doi.org/10.1096/fj.13-233098

Wan, F. J., & Swerdlow, N. R. (1997). The basolateral amygdala regulates sensorimotor gating of acoustic startle in the rat. *Neuroscience*, *76*(3), 715–724. https://doi.org/10.1016/S0306-4522(96)00218-7

Wen, T. H., Lovelace, J. W., Ethell, I. M., Binder, D. K., & Razak, K. A. (2019). Developmental changes in EEG phenotypes in a mouse model of fragile X syndrome. *Neuroscience*, *398*, 126–143. https://doi.org/10.1016/j.neuroscience.2018.11.047

Yuhas, J., Cordeiro, L., Tassone, F., Ballinger, E., Schneider, A., Long, J. M., Ornitz, E. M., & Hessl, D. (2011). Brief report: Sensorimotor gating in idiopathic autism and autism associated with fragile X syndrome. *Journal of Autism and Developmental Disorders*, *41*(2), 248–253. https://doi.org/10.1007/s10803-010-1040-9

SUPPORTING INFORMATION

Additional supporting information can be found online in the Supporting Information section at the end of this article.

How to cite this article: Kat, R., & Kas, M. J. H. (2022). Largely unaffected auditory and visual sensory processing phenotypes in the evoked potentials of Fmr1 KO2 mice. *European Journal of Neuroscience*, *56*(8), 5260–5273. https://doi.org/10.1111/ejn.15808